Phonons in an Entropic Crystal

Zhengdong Cheng,[1,*] Jixiang Zhu,[2] William B. Russel,[2] and P. M. Chaikin[1]
[1]*Department of Physics, Princeton University, Princeton, New Jersey 08540*
[2]*Department of Chemical Engineering, Princeton University, Princeton, New Jersey 08540*
(Received 18 August 1999)

Hard spheres crystallize due to purely entropic forces. The underlying excluded-volume interaction is completely anharmonic and the nature of the phonon spectrum is therefore of interest. To measure the single-particle motion and the phonon spectrum by dynamic light scattering we have used a collection of novel techniques including multispeckle cross correlation on a CCD chip and the growth of large single crystals using a temperature gradient. The random hexagonal close packed crystal has a dispersion relation closer to hcp than to fcc.

PACS numbers: 63.20.–e, 42.25.Fx, 82.70.Dd

In this Letter, we shall report the particle dynamics in a colloidal hard sphere crystal using a novel dynamic light scattering technique. A crystal distinguishes itself from a liquid by possessing a finite shear modulus and a transverse phonon spectrum. Although the crystallization of hard spheres has been intensively studied in the past three decades, investigations have focused on the phase diagram [1,2] and crystallization kinetics [3,4]. Other properties of hard sphere crystals have not been as thoroughly investigated partially due to the lack of large, well-oriented crystal samples and partially due to problems of multiple scattering and nonergodicity. The phonon spectrum for conventional solids is well calculated from force constants (a harmonic approximation) associated with the interparticle potential often evaluated at $T = 0$. Hard spheres interact with a potential which is infinite at contact and zero at any separation and has no analytic derivatives. The free energy is entirely entropic (hence zero at $T = 0$) and long wavelength modes are therefore accessible from thermodynamics. Here we measure the complete phonon spectrum including the short wavelengths at the Brillouin zone edge and find similarity with conventional solids.

The largest hard sphere crystals reported so far are of the order 100 μm on earth and 1 mm in microgravity using 0.5 μm spheres [2]. Recently we developed a temperature gradient technique to control the self-assembly of hard sphere crystals [5] and were able to produce large and well-oriented crystals. Hence so far lattice dynamics are studied only with dilute charged sphere crystals by light scattering [6–8]. On the other hand, for a concentrated system such as a colloidal hard sphere crystal or glass, as well as emulsion, foams, biosystems, etc., the nonergodic character and the extremely slow relaxations challenge the capabilities of conventional dynamic light scattering measurements [9]. Recently, multispeckle autocorrelation spectroscopy techniques were developed [10]. An area detector such as a charge-coupled device (CCD) chip acts as an array of photomultipliers that measure the intensity $I(\mathbf{q}, t)$ for many different $\mathbf{q}$ vectors simultaneously. The time average can thus be replaced by an ensemble average of many correlation functions measured on different pixels with the same $\mathbf{q}$ vector. The correlation function can be measured in real time and the measurement need only last as long as the time scale of interest. For a highly concentrated sample, another challenge is to handle multiple scattering. A novel technique for suppressing multiple scattering by spatial cross correlation was developed recently with an array of two optic fibers to detect the scattering light [11]. Multiple scattering in the sample will illuminate a greater volume of the sample than the incident beam. Since speckle size is inversely related to the dimension of the illuminated volume, multiple scattering produces smaller speckles than the single scattering from the direct incident beam. Scattered light intensity from a sample is correlated only over a speckle size. Therefore taking the cross correlation of pixels within a single-scattering speckle but spaced farther apart than a multiple scattering speckle eliminates the multiple scattering. In our experiment, those two techniques are combined. We used a GBC CCTV CCD camera. The CCD chip has 640 $\times$ 480 pixels. Each pixel square is 12 μm in size. A DT3155 PCI board grabs a series of images. The cross correlation function of the scattering on two pixels that are separated by 5 pixels was calculated and an ensemble average was achieved by averaging over a square of typically 100 $\times$ 100 pixels and 20 separate runs. A dilute sample of strongly scattering polystyrene particles in glycerol (to make the simple diffusion appear nonergodic on the time scale of the experiment) was prepared and measured. The excellent agreement with diffusion constant and correlation function of the Brownian particles served to test and validate our technique.

Figure 1 shows the principle of controlled crystal growth of hard spheres by a temperature gradient. The coexistence region of liquid-crystal transition under each uniform temperature T_1 or T_2 ($T_1 > T_2$) is $0.494 < \phi < 0.545$. Application of a temperature gradient to an initially homogeneous fluid sample with volume fraction ϕ just below freezing generates a gradient in osmotic pressure that will drive particles from the high temperature region to the low temperature region, stimulating controlled nucleation and

 0031-9007/00/85(7)/1460(4)$15.00

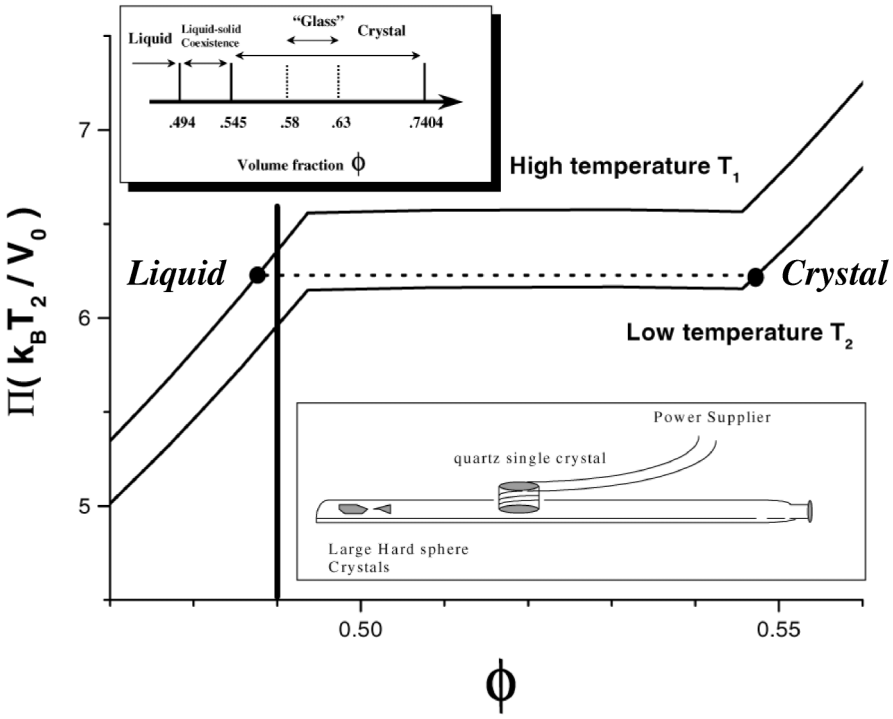

FIG. 1. The effect of a temperature gradient on a hard sphere suspension. Shown are osmotic pressures calculated from Carnahan-Starling and Hall ($\phi_{\max} = 0.74$) equations of state for $T_2 = 300$ K and $T_1 = 320$ K. V_0 is the volume of the sphere. At each uniform temperature, the fluid and crystal coexistence regime is $0.494 < \phi < 0.545$, while under a temperature gradient a high temperature liquid coexists with a low temperature crystal as indicated by the dotted line. The temperature gradient can control the "supercooling" of the metastable fluid, the site of nucleation, and the speed of crystal growth. It is also in principle a powerful tool to investigate the equilibrium hard sphere crystal structure. Upper inset: Equilibrium phase diagram. Bottom inset: Experiment setup.

growth in the low temperature region. We used PMMA particles in a density matching solvent, a decalin and cycloheptyl bromide mixture. In the presence of gravity, convective flow of the solvent established under the temperature gradient will help the macroscopic transport of the PMMA particles. Large hard sphere crystals, 3 mm in size, were thus produced. Figure 2 shows one of the single crystals. The picture was taken by a video camera under conditions where the white light was Bragg reflected. More quantitative Bragg scattering shows the structure of this crystal to be random hexagonal close packing (rhcp) with the close packed planes parallel to the surface of the glass tubing. There were six symmetrically distributed

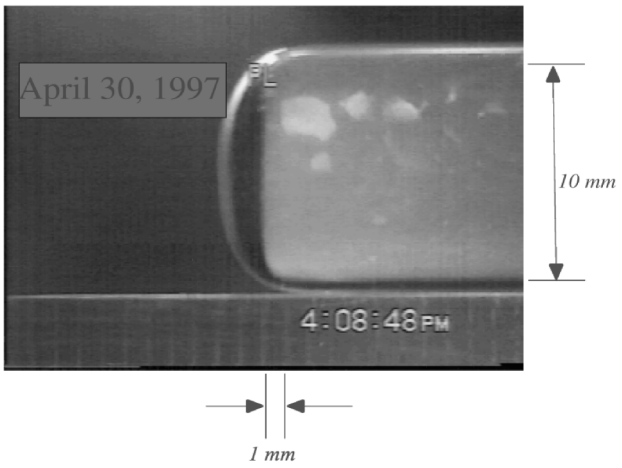

FIG. 2. Single colloidal hard sphere crystals grown by the temperature gradient technique, captured by a video camera. The crystals are about 3 mm in size and have a blocklike shape.

Bragg spots in the forward scattering direction and six Bragg spots in the back scattering direction forming the mirror image of the forward ones corresponding to the hexagonal close packing plane. The nearest neighbor separation in the close packed plane deduced from the Bragg scattering is $r_{\text{nn-c.p.p.}} = 793$ nm, for particles with an initial diameter of 700 nm (slightly swollen by the solvent, 2% in diameter). A good mass density matching between the particle and the solvent reduces the effective gravity to $10^{-3}g$, but a slight refractive index mismatch ($n_{\text{PMMA}} = 1.503$, $n_{\text{solvent}} = 1.498$ at room temperature) remains. The light scattering reported was set up with the incident beam perpendicular to the close packed planes. The forward scattering measurements were conducted from $q \sim 0$ to one of the six Bragg spots.

Large q, large angle scattering is dominated by self-diffusion. Figure 3(a) shows the results measured at 136°. The mean square displacement is constant at long times because the spheres are constrained to the lattice structure. The mean square displacement of a single sphere can be used to characterize the viscoelastic properties of colloidal crystals as done for complex fluids and the gels [12]. Here we just report the value of the Lindemann parameter and estimate of the low frequency elastic modulus. The Lindemann parameter [13] measured is

$$L = |\Delta \mathbf{r}^2_{\max}|^{1/2}/r_{nn} \approx 0.08 \pm 0.01\,.$$

Where r_{nn} is the nearest neighbor separation in the crystal and $|\Delta \mathbf{r}^2_{\max}|^{1/2}$ is the maximum displacement of single sphere. L values of ~0.10 are expected for crystals near the melting point. So the volume fraction of the single

crystal under study was a little bit higher than melting volume fraction 0.545, consistent with the Bragg scattering result.

By equating the thermal energy per sphere ($\frac{3}{2}kT$) to the elastic energy ($\frac{\Delta \mathbf{r}^2_{\max}}{(r_{nn}/2)^2}\ \frac{4\pi a^3/3}{\phi} G_0'$), we estimate the low frequency elastic modulus [12] as $G_0' \approx \frac{9\phi}{32\pi}\frac{kT}{a^3 L^2}$. So the measurement gives $G_0' \approx 0.71 \pm 0.14$ Pa or $\frac{G_0' a^3}{kT} \approx 7.3 \pm 1.3$. This dimensionless value is consistent with the result of a molecular dynamics study on fcc crystals [14] and measurements with charged silica spheres at the liquid-crystal phase boundary (for particles with diameter 238 or 255 nm) [15].

For coherent scattering, the multiphonon expansion of the normalized autocorrelation function $g^{(1)}(\mathbf{q}, t) = F(\mathbf{q}, t)/F(\mathbf{q}, 0)$ is [6],

$$g^{(1)}(\mathbf{q}, t) = e^{-2M}\left[(2\pi)^3 \Omega^{-1} \sum_m \delta^3(\mathbf{q} - \mathbf{K}_m)\right] + \sum_{\Delta q, \nu} (q^\alpha n^{\alpha\nu}_{\Delta q})^2 \langle |Q^\nu_{\Delta q}| \rangle^2 \left[(2\pi)^3 \Omega^{-1} \sum_m \delta^3[\mathbf{q} - (\mathbf{K}_m - \Delta \mathbf{q})] \rho^\nu_{\Delta q}(t)\right] + \ldots .$$

Where M is the Debye-Waller exponent, $\Delta \mathbf{q}$ is the wave vector of the phonon, α the coordinate label, ν polarization, $n^{\alpha\nu}_{\Delta q}$ the amplitude, Ω the volume of the direct-lattice unit cell, and $\rho^\nu_{\Delta q}(t)$ is the time autocorrelation function of the normal mode $Q^\nu_{\Delta q}(t)$. The essential features of the scattering can be seen in the expansion. The first term is the zero-phonon scattering (Bragg scattering) representing elastic scattering that occurs only when $\mathbf{q}$ equals a reciprocal vector $\mathbf{k}_m$. It is reduced in intensity by the Debye-Waller factor. The second term is the one-phonon scattering, which is quasielastic. Only the phonons of the vector $\Delta \mathbf{q}$, where $\Delta \mathbf{q}$ is measured from the nearest reciprocal lattice point, contribute to the scattering into wave vector $\mathbf{q}$. This allows detection of only one mode at a time in the one phonon limit.

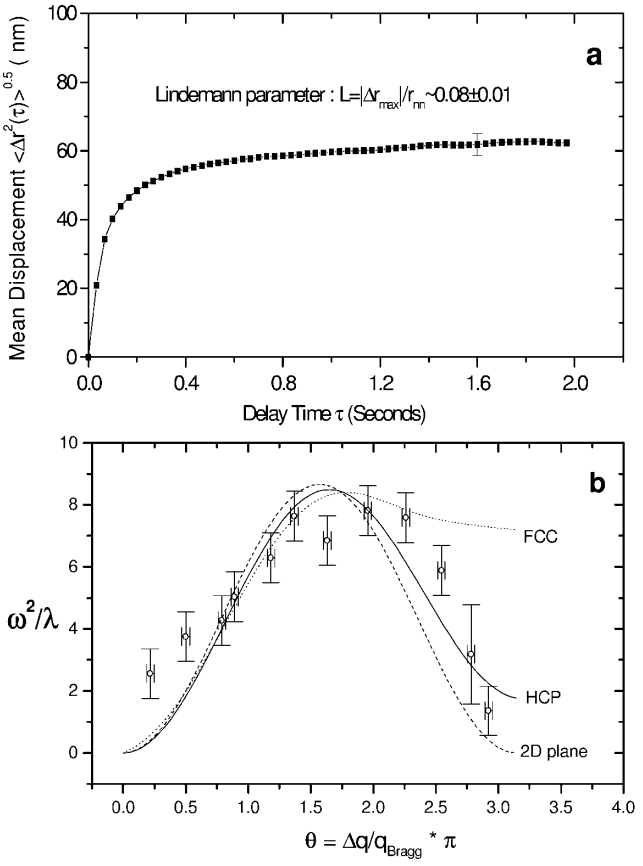

FIG. 3. (a) Single particle mean displacement measured at scattering angle 136°. (b) Phonon dispersion curve. The curves are the central force approximation calculations for fcc and rhcp structures, as well as 2D close packing planes.

Unlike phonons in conventional solids, all but the very low frequency, long wavelength shear modes (transverse phonons) are strongly overdamped from the viscous drag between particle and solvent in colloidal crystals. Thus the correlation function decays exponentially,

$$\rho^\nu_{\Delta q}(t) = \exp\left[-\frac{(\omega^\nu_{\Delta q})^2}{\lambda^\nu_{\Delta q}}\, t\right],$$

with $\omega^\nu_{\Delta q}$ being the eigenvalues of the elastic matrix and $\lambda^\nu_{\Delta q}$ the eigenvalues of the dissipation matrix [6].

The forward scattering has contributions from incoherent scattering (particle self-diffusion) and one phonon scattering. The former has been measured at large angles as described above and is known to have a q^2 dependence. After the subtraction of the self-diffusion part from the measured correlation function, a single-exponential decay was observed for $\rho^\nu_{\Delta q}(t)$ and the fit gave ω^2/λ (Fig. 4). Figure 3(b) shows the dispersion curves named by analogy to atomic systems in the first and second Brillouin zone along the direction from the first Brillouin zone center to one of the Bragg spots.

In the central force harmonic approximation, the longitudinal phonon dispersion in the direction from the center to one of the Bragg spots for hcp structure is

$$m\omega^2 = 6k\left(\sin^2\theta + \frac{2}{9}\sin^2\frac{2\theta}{3} + \frac{1}{9}\sin^2\frac{\theta}{3}\right),$$

where k is the spring constant of the interaction between a pair of spheres, m the mass of the sphere, and $\theta = (\Delta q/q_{\text{Bragg}}) \times \pi$ [16]. For fcc structure, the intended longitudinal mode was mixed with a transverse mode (out of the close packing plane). Figure 3(b) shows the dramatic difference between the measurement for rhcp and the fcc calculation (with admixture between longitudinal

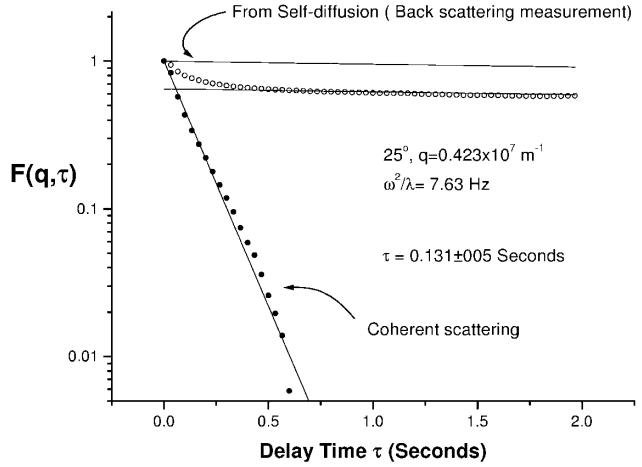

FIG. 4. Extraction of the coherent scattering at the forward scattering angle of 25°. The total correlation was measured by intensities cross-correlation measurements (5-pixel separation) averaging 640 × 160 pixels, accumulating over 15 runs. After subtraction of the self-diffusion, calculated based from the backscattering measurement, a single exponential was fitted to obtain the decay time τ and hence the phonon parameter ω^2/λ.

and transverse modes). On the other hand, the calculation of in-plane motion only (2D planes) obviously underestimates the interaction from neighbor planes, as shown in Fig. 3(b). rhcp data for the phonon modes near the Bragg rods fall between hcp and fcc calculations but closer to the former as one might expect from the closer structural similarity between rhcp and hcp. The finite value of ω^2/λ near the zone center is due to the contribution from the transverse phonons.

The high frequency shear modulus G'_∞ is related to the spring constant as [17] $G'_\infty = 0.83 \times (3/4\pi)^{1/3}\phi^{1/2}k/a$. The drag can be taken to be independent of Δq for longitudinal phonons [6] and estimated [18] as $\lambda \sim \frac{6\pi\eta\beta(\phi)a}{m} \sim \frac{6\pi\eta\times 55\times a}{m}$ with $\eta \sim 2 \times 10^{-3}$ Pa S, and $\beta(\phi)$ correcting for hydrodynamic interaction in the lattice. Therefore, the fit to the data gives $G'_\infty = (1.0 \pm 0.2)$ Pa or $G'_\infty a^3/k_BT \approx 10.4 \pm 1.5$. Notice that $G'_\infty = 1.43G'_0$, which is consistent with a few measurements available [19].

Thus we find, somewhat surprisingly, that the phonon spectrum for these most anharmonic crystals is similar to what we would find for harmonic crystals with the same relationship between the zone boundary (highest frequency) phonon and the long wavelength elastic modulus.

It is interesting to notice the maximum value of ω^2/λ is 2 orders of magnitude smaller than that of charged sphere crystals [6]. This is due to the fact that the shear modulus is much smaller and the friction coefficient is larger for hard sphere crystals, since the charged spheres crystallize at much lower volume fractions and samples can be made much "deeper" into the crystalline phase.

In summary, we have used a novel method, temperature gradient control and density matching, to make large colloidal crystals (~3 mm) for 0.7 μm PMMA/PHSA spheres. The structure of these single crystals is rhcp. We then developed a new dynamic light scattering technique (multispeckle cross-correlation light scattering) to investigate the single particle and lattice dynamics of hard sphere crystals just on the solid side of melting. Despite the presence of the strongly anharmonic hard sphere potential, these entropic crystals have short wavelength phonons with a similar dispersion to conventional materials.

We acknowledge the financial support from NASA Microgravity Sciences Program and useful discussions with Bill Meyer from NASA Glenn Research Center.

*Corresponding author.
Email address: zcheng@princeton.edu, zcheng@erenj.com
Electronic address: www.princeton.edu/~zcheng

[1] P. N. Pusey, in *Liquids, Freezing and Glass Transition*, Proceedings of the Les Houches Summer School, Session 51 (North-Holland, Amsterdam, 1991), Chap. 10; J. P. Hansen, D. Levesque, and J. Zinn-Justin, *Observation, Prediction and Simulation of Phase Transition in Complex Fluids,* edited by W. C-K. Poon, P. N. Pusey, M. Baus, L. F. Rull, and J. P. Ryckaert (Kluwer, Dordrecht, 1995), p. 3.
[2] J. Zhu *et al.*, Nature (London) **387**, 883 (1997); Z. Cheng, P. M. Chaikin, and W. B. Russel, Mater. Des. (to be published).
[3] B. J. Ackerson and K. Schätzel, Phys. Rev. E **52**, 6448 (1995).
[4] Z. Cheng, Ph.D. thesis, Princeton University, 1998, Chap. 5.
[5] Z. Cheng, P. M. Chaikin, and W. B. Russel, Nature (London) **401**, 893 (1999).
[6] A. J. Hurd *et al.,* Phys. Rev. A **26**, 2869 (1982).
[7] J. Derksen and W. van de Water, Phys. Rev. A, **45**, 5660 (1992).
[8] M. Hoppenbrouwers and W. van der Water, Phys. Rev. Lett. **80**, 3871 (1998).
[9] W. van Megen and S. M. Underwood, Phys. Rev. E **49**, 4206 (1994); E. Bartsch, V. Fraanz, and H. Sillescu, J. Non-Cryst. Solids **172**, 88 (1994).
[10] S. Kersch *et al.,* J. Chem. Phys. **104**, 1758 (1996); A. Wong and P. Wiltzius, Rev. Sci. Instrum. **64**, 2547 (1993).
[11] W. V. Meyer *et al.,* Appl. Opt. **36**, 7551 (1997).
[12] T. G. Mason, Hu Gang, and D. A. Weitz, J. Opt. Soc. Am. A **14**, 139 (1997); T. G. Mason and D. A. Weitz, Phys. Rev. Lett. **75**, 2770 (1995).
[13] F. A. Lindemann, Phys. Z. **11**, 609 (1910); J. Bongers and H. Versmold, J. Chem. Phys. **104**, 1519 (1986).
[14] D. Frenkel and A. Ladd, Phys. Rev. Lett. **59**, 1169 (1987).
[15] M. K. Chow and C. F. Zukoski, J. Rheol. **39**, 33 (1995).
[16] N. W. Ashcroft and N. D. Mermin, Solid State Physics (Saunders College Publishing, Fort Worth, Texas, 1976), Chap. 22.
[17] J. W. Goodwin, T. Gregory, and J. A. Stile, Adv. Colloid Interface Sci. **17**, 185 (1982).
[18] S. Kim and W. B. Russel, J. Fluid Mech. **154**, 269 (1985).
[19] See Eng Phan *et al.,* Phys. Rev. E **60**, 1988 (1999).